Title

Metabolic Reprogramming by MYCN Confers Dependence on the Serine-Glycine-One-Carbon Biosynthetic Pathway

Journal

Cancer Research, 79(15)

ISSN

0008-5472

Authors

Xia, Yingfeng
Ye, Bingwei
Ding, Jane
et al.

Publication Date

2019-08-01

DOI

10.1158/0008-5472.can-18-3541

Peer reviewed

HHS Public Access

Author manuscript

Cancer Res. Author manuscript; available in PMC 2020 August 01.

Published in final edited form as:

Cancer Res. 2019 August 01; 79(15): 3837–3850. doi:10.1158/0008-5472.CAN-18-3541.

Metabolic reprogramming by MYCN confers dependence on the serine-glycine-one-carbon biosynthetic pathway

Yingfeng Xia[#1], **Bingwei Ye**[#2], **Jane Ding**[#2], **Yajie Yu**[1], **Ahmet Alptekin**[2], **Muthusamy Thangaraju**[3], **Puttur D. Prasad**[3], **Zhi-Chun Ding**[2,3], **Eun Jeong Park**[2], **Jeong-Hyeon Choi**[7], **Bei Gao**[8], **Oliver Fiehn**[8], **Chunhong Yan**[2,3], **Zheng Dong**[4,6], **Yunhong Zha**[1], **Han-Fei Ding**[2,3,5]

[1]Institute of Neural Regeneration and Repair and Department of Neurology, The First Hospital of Yichang, Three Gorges University College of Medicine, Yichang, 443000, China.

[2]Georgia Cancer Center, Medical College of Georgia, Augusta University, Augusta, Georgia 30912, USA.

[3]Department of Biochemistry and Molecular Biology, Medical College of Georgia, Augusta University, Augusta, Georgia 30912, USA.

[4]Department of Cell Biology and Anatomy, Medical College of Georgia, Augusta University, Augusta, Georgia 30912, USA.

[5]Department of Pathology, Medical College of Georgia, Augusta University, Augusta, Georgia 30912, USA.

[6]Charlie Norwood VA Medical Center, Augusta, GA 30904, USA.

[7]National Marine Bio-Resources and Information Center, National Marine Biodiversity Institute of Korea, Chungchungnam-do 33662, Republic of Korea.

[8]NIH West Coast Metabolomics Center, University of California, Davis, California 95616, USA

[#] These authors contributed equally to this work.

Abstract

MYCN amplification drives the development of neuronal cancers in children and adults. Given the challenge in therapeutically targeting MYCN directly, we searched for MYCN-activated metabolic pathways as potential drug targets. Here we report that neuroblastoma cells with MYCN amplification show increased transcriptional activation of the serine-glycine-one-carbon (SGOC) biosynthetic pathway and an increased dependence on this pathway for supplying glucose-derived carbon for serine and glycine synthesis. Small molecule inhibitors that block this metabolic pathway exhibit selective cytotoxicity to MYCN-amplified cell lines and xenografts by inducing metabolic stress and autophagy. Transcriptional activation of the SGOC pathway in MYCN-amplified cells requires both MYCN and ATF4, which form a positive feedback loop, with MYCN

Corresponding Authors: Yunhong Zha, Department of Neurology, The First Hospital of Yichang, Yichang, 443000, China. Phone: 86-138-7266-2508; yzha7808@ctgu.edu.cn and Han-Fei Ding, Georgia Cancer Center, Augusta University, 1410 Laney Walker Boulevard CN-2151, Augusta, GA 30912, USA. Phone: 706-721-4286; Fax: 706-721-1670; hding@augusta.edu.

Disclosure of Potential Conflicts of Interest

No potential conflicts of interest were disclosed.

Statement: The authors declare no potential conflicts of interest.

activating ATF4 mRNA expression and ATF4 stabilizing MYCN protein by antagonizing FBXW7-mediated MYCN ubiquitination. Collectively, these findings suggest a coupled relationship between metabolic reprogramming and increased sensitivity to metabolic stress, which could be exploited as a strategy for selective cancer therapy.

Introduction

MYCN is a member of the MYC family of oncogenic transcription factors that also include MYC and MYCL. A primary function of MYCN, as well as other MYC family proteins, is to promote cell growth and proliferation through transcriptional regulation (1,2). Aberrant MYCN activation, mainly via genomic amplification, is commonly observed in neuronal and neuroendocrine cancers, including neuroblastoma (3), medulloblastoma (4,5), Wilms tumor (6), retinoblastoma (7), neuroendocrine prostate cancer (8–10), glioblastoma (11,12), and small-cell lung cancer (13–15). However, MYCN is a poor drug target (16). We reasoned that the cell proliferation program driven by MYCN activation might create a selective pressure on metabolic pathways to meet the biosynthetic demand of growth, thereby imposing metabolic dependences that can be exploited therapeutically. Our investigation reveals that MYCN and ATF4, a master regulator of amino acid metabolism and stress responses (17–19), form a positive feedback loop for transcriptional activation of the serine-glycine-one-carbon (SGOC) metabolic pathway. This metabolic reprogramming generates a SGOC pathway-dependent synthetic lethal effect in *MYCN*-amplified neuroblastoma cells. Thus, targeting the SGOC metabolic pathway may provide selective therapeutic benefits for patients with *MYCN*-amplified cancers.

Materials and Methods

Cell Lines and Cell Culture

Neuroblastoma cell lines BE(2)-C (CRL-2268), IMR32 (CCL-127), SH-SY5Y (CRL2266), SK-N-AS (CRL-2137), SK-N-DZ (CRL-2149), SK-N-FI (CRL-2141), and SK-N-SH (HTB-11) were obtained from ATCC, LA1–55n (06041203) from Sigma-Aldrich, and CHLA-90, LA-N-5, LA-N-6, SMS-KANR, and SMS-KCNR from Children's Oncology Group Cell Culture and Xenograft Repository. NBL-S was a gift from S.L. Cohn (University of Chicago), NLF from M.C. Simon (University of Pennsylvania) and SHEP1 from V.P. Opipari (University of Michigan). All cell lines had been authenticated using short tandem repeat profiling (ATCC) and after authentication, large frozen stocks were made to ensure against contaminations by other cell lines. All cell lines were used within 10 passages after reviving from the frozen stocks and were free of *Mycoplasma* contamination as determined by a LookOut Mycoplasma PCR kit (Sigma-Aldrich) and staining cells with DAPI every 3 months. IMR32, SHEP1, SH-SY5Y, SK-N-AS, and SK-N-SH were cultured in DMEM (HyClone SH30022), BE(2)-C in DME/F-12 1:1 (HyClone SH30023), and all others in RPMI 1640 (HyClone SH30027). All culture media were supplemented with 10% FBS (Atlanta Biologicals S11050).

Patient data analyses

The Sequencing Quality Control (SEQC) dataset of MAQC-III was downloaded from the NCBI Gene Expression Omnibus (accession number GSE62564) (20). Kaplan-Meier survival analysis based on the SGOC 6-gene signature (*PHGDH, PSAT1, SHMT2, MTHFD1, MTHFD1L,* and *MTHFD2*) was performed using the software R 3.3.2. Gene expression correlation analyses were conducted online using the R2 Platform (https://hgserver1.amc.nl/cgi-bin/r2/main.cgi), and the resulting figures and *p* values were downloaded. Gene Ontology (GO) analysis of the *MYCN*-amplification gene signature (21) was performed using the software DAVID (22).

Quantitative reverse-transcription PCR (qRT-PCR)

Total RNA was isolated using Trizol (Invitrogen). Reverse transcription was performed using an iScript Advanced cDNA Synthesis Kit (Bio-Rad). qRT-PCR was performed using a 2X SYBR green qPCR master mix (Bimake) on an iQ5 real-time PCR system (Bio-Rad) with gene specific primers (Supplementary Information). All samples were normalized to β2 microglobulin (B2M) mRNA levels.

Overexpression and RNA interference

The Retro-X Tet-Off Advanced Inducible System (Clontech) was used to generate neuroblastoma cell lines with inducible ATF4, FBXW7α or MYCN expression in the absence of doxycycline (Doxy). Human myc-tagged *ATF4* and myc-tagged *FBXW7α* were generated by PCR using pRK-ATF4 (Addgene #26114) and pCR4-TOPO-FBXW7α (Open Biosystems MHS4426–99239216) as templates, respectively. The sequences were verified by sequencing and subcloned into pRetroX-Tight-pur (Clontech) and pCDH-CMV-MCS-EF1-puro (SBI System Biosciences). Lentiviral shRNA constructs shATF4–73 (TRCN0000013573), shATF4–74 (TRCN0000013574), shMYCN-94 (TRCN0000020694), and shMYCN-95 (TRCN0000020695) were obtained from Sigma-Aldrich, shPHGDH (RHS3979–9595900) from Thermo Fisher, and shFBXW7 (RHS4533-NM_001013435) from Open Biosystems. Retroviruses for the expression of ATF4, FBXW7α or MYCN were produced in 293FT cells using the packaging plasmids pHDM-G and pMD.MLVogp (gifts from R. Mulligan at MIT), and lentiviruses for the expression of shRNA, ATF4 or MYCN were produced in 293FT cells using the packaging plasmids pLP1, pLP2, and pLP/VSVG (Thermo Fisher). Retroviral and lentiviral infections of cells were conducted according to standard procedures.

Immunoblotting

Proteins (20–50 μg) were separated on SDS-PAGE, transferred to nitrocellulose membranes, and probed with antibodies (Supplementary Information). Proteins were visualized and quantified using the Odyssey system (LI-COR Biosciences) or a Clarity Western ECL Kit (Bio-Rad) and ImageJ (version 1.50e). Films were exposed for various times for quantification of target proteins within their linear range of detection.

Chromatin immunoprecipitation and quantitative PCR (ChIP-qPCR)

ChIP was performed as described (23) using the cell lines BE(2)-C, SMS-KCNR, SHEP1_pCDH-MYCN, BE(2)-C_shATF4–73, and BE(2)-C_tetoff-ATF4 (± 2 μg/ml Doxy for 6 days). For each antibody, ~4 × 10^7 cells were used. Cross-linked chromatin was sheared through sonication (Fisher Scientific Model 150E) and immunoprecipitated using ChIP grade rabbit anti-ATF4 (sc-200), mouse anti-MYCN (B8.4.B, sc-53993), control mouse IgG (sc-2025) or rabbit IgG (sc-2027) from Santa Cruz Biotechnology. For qPCR, two independent ChIP samples were analyzed, and each sample was assayed in triplicate using ChIP-qPCR primers (Supplementary Information). The number associated with each primer set indicates the position of the forward primer relative to its target gene transcription start site (TSS, +1).

MYCN half-life assay

BE(2)-C_tetoff-ATF4 and SK-N-DZ_tetoff-ATF4 cells were cultured with or without 2 μg/ml Doxy for 5 days, followed by addition of cycloheximide to a final concentration of 10 μg/ml. Samples were then collected at various time points for immunoblot analysis of MYCN protein levels, which were quantified against β-actin using ImageJ.

In vivo ubiquitination assay

The assay was performed as described (24). Briefly, BE(2)-C cells were co-transfected with pFlag-CMV-2-ubiquitin and pcDNA3.1-FBXW7α, along with or without pCDH-ATF4, and BE(2)-C cells expressing shGFP, shATF4–73, shFBXW7–55 or both shATF4–73 and shFBXW7–55 were transfected with pFlag-CMV-2-ubiquitin. Approximately 44 h after transfection, cells were treated with 10 μM MG-132 for 4 h, washed with PBS and lysed with a lysis buffer containing 2% SDS, 150 mM NaCl, 10 mM Tris-HCl, (pH 8.0), 2 mM sodium orthovanadate, and 50 mM sodium fluoride. The lysates were boiled for 10 min, sonicated (Fisher Scientific Model 150E, amplitude 40 and time 10 sec), and diluted 1:10 with a dilution buffer (10 mM Tris-HCl, pH 8.0, 120 mM NaCl, and 1% Triton-X 100), followed by MYCN immunoprecipitation with mouse anti-MYCN (B8.4.B) and Protein G Dynabeads (ThermoFisher 10003D) and immunoblotting using rabbit anti-Flag for Flag-ubiquitin (Sigma-Aldrich F-7425) and rabbit anti-MYCN (Cell signaling #9405).

Inhibitor assays

Small molecule inhibitors NCT-503 (Sigma-Aldrich SML1659), NCT-503 inactive control (Sigma-Aldrich SML1671), and CBR-5884 (Sigma-Aldrich SML1656) were dissolved in dimethyl sulfoxide (DMSO), and stock solutions were aliquoted and stored at −80°C until use. Cells were treated with DMSO, NCT-503 or CBR-5884 for 2–3 days, and the number of viable cells was determined by trypan blue exclusion assay. To assess the effect of supplemental serine on NCT-503 action, cells were cultured in MEM (Gibco 11095–080) supplemented with 10% dialyzed FBS (Gibco 26400–044), 4.5 g/L D-(+)-glucose (Sigma-Aldrich G8769), 1x MEN vitamins (Gibco 11120–052), 1x sodium pyruvate (Gibco 11360–070), and non-essential amino acids alanine, asparagine, glutamic acid, glycine, proline with or without 0.4 mM serine.

Amino acid uptake assay

[^{3}H]-Glycine (60 Ci/mmol) and [^{3}H]-Serine (11 Ci/mmol) were purchased from Moravek. Cells in 24-well plates were washed twice with the transport buffer (25 mM HEPES/Tris, pH 7.5, 140 mM NaCl, 5.4 mM KCl, 1.8 mM $CaCl_2$, 0.8 mM $MgSO_4$, and 5 mM glucose). Transport of 5 μM glycine or serine (0.05 μM [^{3}H]-glycine or [^{3}H]-serine plus 4.95 μM unlabeled glycine or serine) was measured at 37°C for 2.5, 5.0, 10, and 15 min. Transport was terminated by aspiration of the transport buffer followed by three washes with 2 ml of ice-cold transport buffer. The cells were lysed with 0.5 ml of 1% SDS in 0.2 N NaOH and the radioactivity was determined by scintillation counting.

Metabolomics analysis

SHEP1-pCDH and SHEP1-pCDH-MYCN cells were washed with 5% mannitol and extracted with HPLC grade methanol (ThermoFisher A452–4) containing internal standards according to the instructions provided by Human Metabolome Technologies (HMT). Extracted metabolites were analyzed by Capillary Electrophoresis Time-of-Flight Mass Spectrometry (CE-TOFMS) at HMT. Peaks were annotated with putative metabolites from the HMT metabolite database based on their MTs/RTs and *m/z* values determined by TOFMS. The tolerance range for the peak annotation was configured at ±0.5 min for MT and ±10 ppm for *m/z*. Peak areas were normalized against the internal standards and then the cell number. Three biological replicate samples (~10^6 cells/sample) were analyzed for each cell type and *p* values were calculated by Welch's *t*-test.

Stable isotope flux analysis

BE(2)-C and SK-N-AS cells were cultured in glucose-deficient DMEM (11966–025, Invitrogen) supplemented with 10% dialyzed FBS and 20 mM [U-^{13}C]glucose (CLM-1396, Cambridge Isotope Laboratories) in the presence of DMSO or 10 μM NCT-503 for 24 h. Cells were collected by scraping and centrifugation, and cell pellets were washed once with ice-cold PBS, snap frozen in liquid nitrogen, and stored at −80°C until analysis. Four to six biological replicate samples (~5 × 10^6 cells/sample) were analyzed for each condition and cell type. Metabolite extraction and deprivation, instrumentation, and data processing are described in Supplementary Information.

Microarray

Total RNA was isolated using Trizol from three biological replicates of BE(2)-C cells treated with DMSO or 10 μM NCT-503 for 48 h. Affymetrix microarray was performed using the Human Gene 2.0 ST microarray chip. Data were normalized, significance determined by ANOVA, and fold change calculated with the Partek Genomics Suite. GO analysis was performed with DAVID (22) for all differentially expressed genes (≥ ±1.5 fold, $P < 0.05$), and GSEA was performed as described (25). The NCBI Gene Expression Omnibus (GEO) accession number for the microarray data is GSE120347.

Xenograft assay

BE(2)-C and SK-N-AS cells in 200 μl serum-free DMEM were injected subcutaneously into both flanks of 6-week-old male and female NOD.SCID mice at 2.5 × 10^6 cells per injection

site. Tumor volume was measured every other day using a digital caliper and estimated using the equation $V = (L \times W^2)/2$. Mice bearing tumors of ~100 mm^3 were randomly divided into 2 groups (5 per group), stratified by gender and tumor volume, and treated with vehicle (40 μl DMSO) or 64 mg/kg (body weight) NCT-503 delivered daily by intraperitoneal injection for 10 days. Animals were euthanized when their tumors reach ~1.0 cm in diameter. The animal experiments were approved by the Institutional Animal Care and Use Committee of Medical College of Georgia, Augusta University.

Statistics

Quantitative data are presented as mean ± SD and were analyzed for statistical significance by unpaired, two-tailed Student's *t*-test or two-way ANOVA. PHGDH inhibitor dose-response curves were fitted with the four-parameter equation 'log (inhibitor) vs. response – variable slope' and box plots were generated using the box and whiskers (Turkey) plot. For xenograft study, log-rank test was used to account for mouse survival. Unless otherwise stated, all statistical analyses were conducted using GraphPad Prism 7.0d for Mac.

Additional methods

Additional methods are provided in Supplementary Information.

Results

High expression of the SGOC gene signature is associated with neuroblastoma with *MYCN* amplification

High-risk neuroblastoma is a leading cause of pediatric cancer deaths, and *MYCN* amplification has a major role in its development (2,26–28). To search for potential MYCN-dependent metabolic pathways, we performed gene ontology (GO) analysis of the *MYCN*-amplification gene signature consisting of 143 genes upregulated in neuroblastoma tumors with *MYCN* amplification relative to those without (21). This analysis identified serine-glycine synthesis, one-carbon metabolism, and purine nucleotide biosynthesis as the most significantly upregulated metabolic processes in *MYCN*-amplified neuroblastoma (Fig. 1A). These metabolic processes are connected by the SGOC pathway (Fig. 1B) (29,30). Indeed, the *MYCN*-amplification gene signature contains several genes encoding enzymes within the SGOC pathway (21), including phosphoglycerate dehydrogenase (PHGDH), phosphoserine aminotransferase 1 (PSAT1), mitochondrial serine hydroxymethyltransferase 2 (SHMT2), cytosolic methylenetetrahydrofolate dehydrogenase, cyclohydrolase and formyltetrahydrofolate synthetase 1 (MTHFD1), and mitochondrial methylenetetrahydrofolate dehydrogenase 2 (MTHFD2). These enzymes link the glycolytic intermediate 3-phosphoglycerate (3PG) to the production of serine, glycine, and the one-carbon carriers 5,10-methylene-tetrahydrofolate (5,10-MTHF) and 10-formyl-THF (Fig. 1B). Both glycine and 10-formyl-THF donate carbon, and glycine also contributes nitrogen, moieties for purine nucleotide synthesis; 5,10-MTHF is essential for de novo thymidylate production as a coenzyme of thymidylate synthase.

We further assessed the correlation between *MYCN* amplification and transcriptional reprogramming of SGOC metabolism in neuroblastoma by analyzing the gene expression

profiling data from a cohort of neuroblastoma patients (n = 498, the SEQC dataset) (20). The average expression of the 6 SGOC genes (*PHGDH, PSAT1*, *SHMT2, MTHFD1, MTHFD1L,* and *MTHFD2*) was significantly higher in high-risk tumors with *MYCN* amplification compared to low-risk tumors and to high-risk tumors without *MYCN* amplification (Fig. 1C). We confirmed the observation by analyzing the expression of individual SGOC genes in neuroblastoma tumors with or without *MYCN* amplification (Supplementary Fig. S1A). In agreement with the findings from tumors, *MYCN*-amplified neuroblastoma cell lines expressed markedly higher levels of PHGDH protein in comparison with non-*MYCN*-amplified cell lines (Fig. 1D). This PHGDH expression pattern is specifically associated with *MYCN* amplification but is not a general feature of rapidly proliferating neuroblastoma cell lines as the non-*MYCN*-amplified cell lines SK-N-AS, SK-N-FI, and SHEP1, despite their low PHGDH expression (Fig. 1D), proliferated at similar or faster rates in comparison with the *MYCN*-amplified cell lines BE(2)-C, SK-N-DZ, and SMS-KCNR as determined by cell population doubling time (Supplementary Fig. S1B). Moreover, inhibition of the proliferation of neuroblastoma cell lines by serum deprivation did not reduce PHGDH protein expression (Supplementary Fig. S1C-D). Overexpression of PHGDH in non-*MYCN*-amplified cells had no significant impact on cell proliferation (Supplementary Fig. S1E-F).

Further analysis of the SEQC dataset revealed that higher expression of the SGOC gene signature is significantly associated with advanced stages of neuroblastoma and poor prognosis in neuroblastoma patients (Fig. 1E-F). Together, these findings provide genetic evidence for transcriptional activation of the SGOC metabolic pathway in high-risk neuroblastoma with *MYCN* amplification.

MYCN transcriptionally activates SGOC metabolism

We next investigated whether MYCN is required for transcriptional activation of the SGOC genes. MYCN knockdown by shRNA in *MYCN*-amplified neuroblastoma cell lines reduced mRNA and protein expression of the SGOC genes (Fig. 2A-B and Supplementary S2A). Thus, MYCN has a major role in maintaining steady-state expression of the SGOC genes in these cell lines. In addition, MYCN depletion inhibited cell proliferation and induced differentiation characterized morphologically by neurite outgrowth (Supplementary Fig. S2B-C).

We next investigated whether an increase in MYCN level is sufficient to activate SGOC gene transcription. MYCN overexpression in non-*MYCN*-amplified neuroblastoma cell lines increased expression of the SGOC genes at the mRNA and protein levels (Fig. 2C-F) and enhanced cell proliferation (Supplementary Fig. S2D). Metabolomic profiling of non-*MYCN*-amplified SHEP1 cells with or without MYCN overexpression revealed that MYCN overexpression resulted in a significant increase in the intracellular levels of serine and glycine (Supplementary Fig. S2E) but had no effect on serine and glycine transport (Supplementary Fig. 2F), suggesting that MYCN overexpression enhanced biosynthetic activity of the SGOC metabolic pathway.

To determine whether MYCN directly targets the SGOC genes for transcriptional activation, we performed ChIP-qPCR assays. MYCN and other members of the MYC family bind to

the consensus E-box sequence CANNTG. We focused on *PHGDH, PSAT1, MTHFD1L,* and *MTHFD2*, which contain the canonical E-box sequence CACGTG in their promoters or first introns (Fig. 2G). ChIP-qPCR analysis of the *MYCN*-amplified BE(2)-C cells showed significant levels of endogenous MYCN associated with the E-box sequences (Fig. 2H). We also detected significant levels of MYCN in the proximal promoter regions of *PHGDH, PSAT1, MTHFD1L,* and *MTHFD2* (Fig. 2I). We obtained essentially the same results with the *MYCN*-amplified SMS-KCNR cells (Supplementary Fig. S2G-H) and the non-*MYCN*-amplified SHEP1 cells with MYCN overexpression (Supplementary Fig. S2I). Collectively, these findings suggest that the SGOC genes are direct transcriptional targets of MYCN.

ATF4 is a transcriptional activator of the SGOC genes in *MYCN*-amplified cells

ATF4 has a major role in transcriptional activation of enzymes within the serine-glycine synthesis pathway (31–35). Also, it has been shown recently that ATF4 acts downstream of mTORC1 and NRF2 in transcriptional activation of one-carbon flux and nucleotide biosynthesis (36,37). Given the above findings on MYCN, we wondered if ATF4 has a significant role in transcriptional regulation of the SGOC genes in *MYCN*-amplified cells. Analysis of the SEQC dataset revealed a strong positive correlation in mRNA expression levels between *ATF4* and the SGOC genes, except for *PSPH* and *SHMT1* (Supplementary Fig. S3A). Overexpression of ATF4 in both *MYCN*-amplified and non-*MYCN*-amplified cell lines increased SGOC gene expression at the mRNA and protein levels (Fig. 3A-B and Supplementary Fig. S3B-C). Conversely, ATF4 depletion by shRNA in *MYCN*-amplified cell lines markedly decreased mRNA and protein expression of the SGOC genes (Fig. 3C-D) and inhibited cell proliferation (Supplementary Fig. S3D). Interestingly, ATF4 overexpression had no significant effect on the proliferation of non-*MYCN*-amplified cell lines (Supplementary Fig. S3E) but significantly enhanced the proliferation of *MYCN*-amplified cell lines (Supplementary Fig. S3F), suggesting that ATF4 might cooperate with MYCN in driving cell proliferation. Collectively, these findings indicate an essential role of ATF4 in maintaining SGOC gene expression and sustaining the proliferation of *MYCN*-amplified neuroblastoma cells.

To determine whether ATF4 directly targets the SGOC genes in *MYCN*-amplified cells, we performed ChIP-qPCR analysis of BE(2)-C_tetoff-ATF4 cells. In the absence of induction of exogenous ATF4, significant levels of endogenous ATF4 were found at the promoters of *PHGDH, PSAT1, SHMT2, MTHFD1L,* and *MTHFD2*, as well as those of *ASNS* and *DDTI3*, two classic ATF4 target genes (38,39) (Fig. 3E). Induction of ATF4 further increased the levels of ATF4 at these sites, except for the *MTHFD2* promoter (Fig. 3E). In addition, ATF4 knockdown completely abolished the binding of endogenous ATF4 to the promoters of *PSAT1, MTHFD2,* and *DDIT3* (Supplementary Fig. S3G). Thus, the SGOC genes are direct transcriptional targets of ATF4.

ATF4 is a direct target gene of MYCN and is required for MYCN induction of SGOC genes

Since both MYCN and ATF4 are required for transcriptional activation of the SGOC genes in *MYCN*-amplified cells, we investigated how they coordinate their activities in this process. Analysis of the SEQC dataset revealed significantly higher *ATF4* mRNA levels in tumors with *MYCN* amplification than those without (Supplementary Fig. S4A) and a

positive correlation in mRNA expression levels between *ATF4* and *MYCN* (Supplementary Fig. S4B), suggesting that one might regulate the expression of the other or that both are transcriptionally regulated by a common mechanism. To test these models, we examined the abilities of ATF4 and MYCN to regulate the expression of each other. ATF4 overexpression had no significant effect on *MYCN* mRNA expression (Fig. 4A), whereas MYCN overexpression significantly upregulated mRNA and protein expression of ATF4 (Fig. 4B-C). In addition, MYCN knockdown led to a significant reduction in ATF4 mRNA and protein levels (Fig. 4D-E). Thus, MYCN is a key transcriptional activator of ATF4 expression in neuroblastoma cells.

The ATF4 gene contains two canonical E-box sequences (CACGTG), one in the first intron (+767) and the other in the 3' region (+3915). ChIP-qPCR analysis demonstrated significant levels of endogenous MYCN binding to these regions (Figure 4F, ATF4p_+687 and ATF4p_+3818). In addition, we detected significant levels of MYCN at the *ATF4* promoter 5' region (Fig. 4F). Thus, *ATF4* is a direct target gene of MYCN.

Collectively, these observations suggest that ATF4 functions downstream of MYCN in transcriptional activation of the SGOC genes. In support of this model, ATF4 knockdown significantly abrogated the ability of MYCN to induce the SGOC genes (Fig. 4G), indicating an essential role of ATF4 in mediating transcriptional activation of the SGOC genes by MYCN.

ATF4 stabilizes MYCN protein

During our ChIP-qPCR studies with BE(2)-C_tetoff-ATF4 cells (Fig. 3E), we unexpectedly observed that following ATF4 induction, there was a significant increase in MYCN levels at the promoters of the SGOC genes (Fig. 5A) and *ATF4* (Supplementary Fig. S4C). It has been shown previously that elevated levels of MYC lead to increased MYC occupancy at the promoters of active genes (40,41). Because ATF4 had no effect *MYCN* mRNA expression (Fig. 4A), we asked whether it affects MYCN protein expression. Immunoblotting revealed that ATF4 overexpression increased MYCN protein levels (Fig. 5B), whereas ATF4 knockdown reduced MYCN protein expression (Fig. 5C) and increased MYCN protein ubiquitination (Fig. 5D), leading to a decrease in MYCN occupancy at the SGOC gene promoters (Supplementary Fig. S4D). Moreover, ATF4 overexpression resulted in an average of 2.5-fold increase in MYCN protein half-life (Fig. 5E-F). Collectively, these data suggest that ATF4 increases MYCN protein levels by blocking its degradation.

FBXW7 is a component of the SKP1/CUL1/FBXW7 E3 ubiquitin ligase complex that targets MYCN for proteasomal degradation (42,43). As expected, we found that FBXW7 overexpression markedly reduced MYCN protein levels in *MYCN*-amplified cells (Fig. 5G and Supplementary Fig. S4E), leading to decreased protein levels of SGOC enzymes (Supplementary Fig. S4E). ATF4 overexpression was sufficient to neutralize the effect of FBXW7, leading to increased MYCN protein expression (Fig. 5G) and reduced MYCN protein ubiquitination (Fig. 5H). Conversely, FBXW7 depletion, which had no effect on MYCN mRNA expression (Supplementary Fig. S4F), significantly increased MYCN protein expression, leading to higher PHGDH expression (Fig. 5I). Moreover, when FBXW7 expression was silenced, ATF4 knockdown could no longer increase MYCN protein

ubiquitination (Fig. 5J). Thus, both overexpression and knockdown studies suggest that ATF4 stabilizes MYCN protein by antagonizing FBXW7-mediated MYCN ubiquitination and subsequent degradation. These findings, along with those showing that MYCN transcriptionally activates ATF4 expression (Fig. 4B-C), provide evidence for a MYCN-ATF4 positive feedback loop for transcriptional activation of the SGOC metabolic pathway in *MYCN*-amplified cells.

MYCN sensitizes neuroblastoma cells to PHGDH inhibition

The observation that the SGOC genes are transcriptionally activated in *MYCN*-amplified relative to non-*MYCN*-amplified neuroblastoma cells led us to hypothesize that inhibition of this metabolic pathway might be synthetically lethal with *MYCN* amplification. We tested this hypothesis in a panel of neuroblastoma cell lines with *MYCN* amplification (BE(2)-C, LA1–55n, SK-N-DZ, and SMS-KCNR) or without (NBL-S, SHEP1, SH-SY5Y, SK-N-AS, and SK-N-FI). Of note, BE(2)-C and SMS-KCNR cells were derived from relapsed tumors after chemotherapy (44) and, as expected, both cell lines were highly resistant to the chemotherapy drug doxorubicin in comparison with the non-*MYCN*-amplified cell lines SK-N-AS, SK-N-FI, and SH-SY5Y and the *MYCN*-amplified cell lines LA1–55n and SK-N-DZ (Fig. 6A).

We treated these cell lines with NCT-503, a small molecule inhibitor of PHGDH (45). NCT-503 (EC_{50} = 8–16 μM) at 10–20 μM markedly inhibited the growth and survival of *MYCN*-amplified cell lines, including the chemoresistant BE(2)-C and SMS-KCNR cells, but had no significant or only a modest effect on non-*MYCN*-amplified cell lines (Fig. 6B-C and Supplementary Fig. S5A). This effect of NCT-503 was neither a result of nonspecific inhibition of MYCN expression (Supplementary Fig. S5B) nor dependent on the proliferation state since serum deprivation, which markedly inhibited the proliferation of both non-*MYCN*- and *MYCN*-amplified cell lines (Supplementary Fig. S1C), had no significant effect on the differential sensitivities of non-*MYCN*- and *MYCN*-amplified cell lines to NCT-503 (Supplementary Fig. S5C). Treatment with NCT-503 negative control compound showed no significant effect on all the cell lines examined.

Consistent with the previous report (45), we observed the growth-inhibiting effect of NCT-503 in the presence (Fig. 6B) or absence (Fig. 6C) of supplemental serine. In addition, non-*MYCN*-amplified (resistant) SK-N-AS cells and *MYCN*-amplified (sensitive) BE(2)-C cells showed no difference in their ability to uptake glycine, whereas BE(2)-C cells displayed a slightly higher activity in transporting serine (Supplementary Fig. S5D). Moreover, NCT-503 treatment modestly inhibited glycine and serine transport of SK-N-AS cells but had no effect on BE(2)-C cells (Supplementary Fig. S5E). Together, these findings suggest that serine and glycine transport is not a major factor in determining the sensitivity of non-*MYCN*- and *MYCN*-amplified cell lines to NCT-503.

We confirmed the sensitivity of *MYCN*-amplified neuroblastoma cells to PHGDH inhibition in parallel studies with another small molecule inhibitor of PHGDH, CBR-5884 (46). Compared with non-*MYCN*-amplified cell lines, *MYCN*-amplified cell lines were also significantly more sensitive to 15–30 μM CBR-5884 (Fig. 6D). In addition, *MYCN*-amplified BE(2)-C and SMS-KCNR cells were significantly more sensitive to PHGDH

knockdown than non-*MYCN*-amplified SHEP1 and SK-N-FI cells (Supplementary Fig. S5F-G). Importantly, MYCN overexpression was sufficient to sensitize non-*MYCN*-amplified SHEP1 and NBL-S cells to NCT-503 (Fig. 6E and Supplementary Fig. S5H).

We next evaluated NCT-503 anti-tumor activity in mouse xenograft models established with *MYCN*-amplified BE(2)-C cells and non-*MYCN*-amplified SK-N-AS cells. Tumor-bearing mice were treated with vehicle or 64 mg/kg (body weight) of NCT-503 by daily intraperitoneal injection for 10 days or until sacrifice. NCT-503 treatment significantly reduced the growth *MYCN*-amplified BE(2)-C xenografts (Fig. 6F, BE(2)-C), and prolonged the survival of tumor-bearing mice (Fig. 6G, BE(2)-C). By contrast, NCT-503 treatment of mice bearing non-*MYCN*-amplified SK-N-AS xenografts showed no significant effect on tumor growth and mouse survival (Fig. 6F-G, SK-N-AS). In all cases, NCT-503 treatment at the indicated dose and time had no significant effect on mouse body weight (Supplementary Fig. S5I).

Collectively, these findings suggest that increased MYCN expression in neuroblastoma cells imposes a dependence on the SGOC metabolic pathway for survival and proliferation.

PHGDH inhibition triggers metabolic stress in *MYCN*-amplified cells

The SGOC pathway links glycolysis to the production of serine, glycine, and one-carbon units. To elucidate the metabolic basis for the differential sensitivities of *MYCN*-amplified and non-*MYCN*-amplified cells to NCT-503, we performed stable isotope flux analysis of glucose carbon into serine and glycine synthesis (Fig. 7A). NCT-503 treatment significantly reduced the production of m+3 serine and m+2 glycine from [U-^{13}C]glucose in *MYCN*-amplified BE(2)-C cells (Fig. 7B-C, DMSO vs. NCT-503). By contrast, no such an effect was observed in non-*MYCN*-amplified SK-N-AS cells (Fig. 7B-7C). Importantly, the proportions of serine and glycine derived from [U-^{13}C]glucose (m+3/m+0 serine and m+2/m+0 glycine) were significantly higher in BE(2)-C cells relative to SK-N-AS cells (Fig. 7B-C, BE(2)-C vs. AS). Taken together, these data indicate that *MYCN*-amplified cells rely more on glucose-derived carbon for serine and glycine synthesis in comparison with non-*MYCN*-amplified cells, suggesting a metabolic basis for their differential sensitivities to PHGDH inhibition.

To gain a molecular understanding for the selective cytotoxic effect of NCT-503 on *MYCN*-amplified cells, we performed microarray gene expression profiling of BE(2)-C cells treated with DMSO or 10 μM NCT-503. A total of 3655 NCT-503-responsive genes (≥ ±1.50 fold, $p < 0.05$) were identified, with 1223 genes being upregulated and 2432 genes downregulated (Supplementary Table S1). GO analysis revealed that genes downregulated by NCT-503 treatment were highly enriched for GO terms associated with DNA replication and G1 to S phase transition (Supplementary Fig. S6A and Table S2). We obtained essentially the same result with gene set enrichment analysis (GSEA), which showed downregulation of a large number of genes involved in DNA replication and G1/S cell cycle transition (Supplementary Fig. S6B). As reported previously (45), NCT-503 treatment induced G1 arrest (Supplemental Fig. S6C), consistent with a key role of the SGOC pathway in supplying nucleotides for DNA replication.

For genes upregulated by NCT-503 treatment, GO analysis showed a significant enrichment for GO terms associated with various stress responses, including glucose starvation, endoplasmic reticulum stress and the unfolded protein response, and oxidative stress (Fig. 7D and Supplementary Table S2). Similarly, GSEA revealed that genes involved in the amino acid deprivation response were most significantly enriched and upregulated (Fig. 7E and Supplementary Fig. S6D). These stress-responsive genes, including *ASNS*, *ASS1, ATF3, CTH, DDIT3, TRIB3*, and *XBP1* (Supplementary Fig. S6D and Tables S1-2), are induced by ATF4 in response to various stress signals (19). In addition, several genes within the SGOC pathway were induced by NCT-503, including *PHGDH, PSAT1, SHMT2,* and *MTHFD2* (Supplementary Table S1). These data suggest that in *MYCN*-amplified cells, NCT-503 treatment elicited an adaptive response to metabolic stress induced by inhibition of SGOC synthesis.

We verified the microarray data by qRT-PCR and immunoblotting, which showed that NCT-503 treatment markedly induced mRNA and protein expression of ATF4, DDIT3 (also known as CHOP) and/or TRIB3 in *MYCN*-amplified, but not in non-*MYCN*-amplified, cell lines (Fig. 7F-G and Supplementary S6E). Overexpression of MYCN, which sensitized non-*MYCN*-amplified cells to NCT-503 (Fig. 6E), was sufficient to confer NCT-503 induction of *ATF4, DDIT3* and *TRIB3* in non-*MYCN*-amplified SHEP1 cells (Fig. 7F). Moreover, NCT-503 treatment induced autophagy in *MYCN*-amplified cells, but not in non-*MYCN*-amplified cells, as evidenced by increased LC3B-II production and the formation of LC3B-positive puncta (Fig. 7H-I and Supplementary Fig. S6F). Together, these findings suggest that PHGDH inhibition induces metabolic stress in *MYCN*-amplified neuroblastoma cells, leading to G1 arrest and autophagy.

Discussion

Our study reveals a MYCN-dependent vulnerability to suppression of the SGOC metabolic pathway. PHGDH inhibition triggered cell cycle arrest and a metabolic stress response with autophagy in *MYCN*-amplified neuroblastoma cells, but not in non-*MYCN*-amplified cells. This increased sensitivity to PHGDH inhibition can be recapitulated by overexpression of MYCN in non-*MYCN*-amplified cells. Mechanistically, we show that in comparison with non-*MYCN*-amplified cells, *MYCN*-amplified cells, likely owing to their higher expression of PHGDH and other SGOC pathway enzymes, have an increased dependence on glucose-derived carbon for the synthesis of serine and glycine (and possibly also one-carbon units as suggested previously (45)). In addition, a recent study showed that PHGDH inhibition in cells with high PHGDH expression could disrupt central carbon metabolism (47), which may help to explain the failure of supplemental serine to rescue the cytotoxic effect of NCT-503. Collectively, these findings suggest a metabolic basis for the differential sensitivities of *MYCN*-amplified and non-*MYCN*-amplified neuroblastoma cells to PHGDH inhibitors.

MYCN amplification has a major role in the development of high-risk neuroblastoma, a leading cause of pediatric cancer deaths (2,26–28). However, targeting MYCN directly for therapy has proved to be challenging (16). An alternative strategy is to target metabolic pathways that are activated by MYCN for sustaining cancer cell growth and proliferation. In

support of this idea, we found that blocking SGOC metabolism selectively inhibits the proliferation and survival of *MYCN*-amplified neuroblastoma cells. Also, a recent study reported that *MYCN*-amplified neuroblastomas display increased folate dependence and are more sensitive to methotrexate, an inhibitor of dihydrofolate reductase that functions to maintain the folate-one-carbon loop for thymidylate synthesis (48). Together, these findings suggest that targeting MYCN-activated metabolic pathways could be a selective therapeutic strategy against *MYCN*-amplified tumors. In addition, our findings have implications in treatment of patients with relapsed neuroblastomas carrying *MYCN*-amplification. Although a majority of patients with high-risk neuroblastoma respond to initial therapy, approximately half of them will eventually have a relapse with resistant to further therapies (27). Currently, there are no effective treatment regimens for these patients. We found that PHGDH inhibitors are effective in inhibiting the growth of chemoresistant BE(2)-C and SMS-KCNR cells and of BE(2)-C xenograft tumors. Both BE(2)-C and SMS-KCNR cell lines were derived originally from relapsed tumors after chemotherapy (44). Thus, blocking SGOC metabolism might provide a treatment strategy for relapsed neuroblastomas with *MYCN* amplification.

ATF4 is a master regulator of amino acid metabolism and stress responses (17–19). We found that MYCN binds to the promoter of *ATF4* to increase its mRNA expression. In addition, we show that MYCN-mediated transcriptional activation of SGOC pathway enzymes requires ATF4. Interestingly, a recent study reported that both MYCN and ATF4 can directly activate the transcription of *ASCT2* (also known as *SLC1A5*), which encodes a glutamine transporter. It also reported a positive correlation in mRNA expression among *MYCN*, *ATF4*, and *ASCT2* in high-risk neuroblastomas, suggesting a potential coordination between MYCN and ATF4 in regulation of ASCT2 expression (49). These findings, along with ours, provide evidence for MYCN and ATF4 to regulate a common set of genes in metabolic reprogramming in neuroblastoma. Our study further uncovers a MYCN-ATF4 positive feedback loop: MYCN transcriptionally activates ATF4 expression, and ATF4 stabilizes MYCN protein by antagonizing FBXW7-mediated MYCN ubiquitination and degradation. This positive feedback loop may be hardwired into *MYCN*-amplified cancer cells to reinforce the hyperactive state of SGOC gene transcription and to boost production outputs of the metabolic pathway required by the MYCN-driven growth program. The ability of ATF4 to stabilize MYCN protein also suggests a molecular mechanism for the observation that ATF4 overexpression significantly enhanced the proliferation of *MYCN*-amplified neuroblastoma cells but had no effect on the proliferation of non-*MYCN*-amplified neuroblastoma cells.

Given the key role of ATF4 as a master regulator of stress responses, our identification of the MYCN-ATF4 positive feedback loop suggests a molecular mechanism for the stress sensitive phenotype of *MYCN*-amplified cancer cells. The feedback loop transcriptionally amplifies SGOC biosynthesis to sustain cell growth and proliferation, but, at the same time, confers to these cells an increased dependence on the SGOC pathway and an intensified stress response to PHGDH inhibition. This is reminiscent of the earlier findings that some oncogenes, such as MYC and E2F1, simultaneously promote cell proliferation and sensitize cells to apoptosis (50). Thus, there might be a coupled relationship between metabolic reprogramming and sensitization to metabolic stress. The notion that cancer cells reprogram

their metabolism to meet the biosynthetic challenge of growth and proliferation but, as a result, are inherently sensitive to metabolic stress may offer numerous opportunities for manipulating cell metabolism in the direction of cancer therapy.

Supplementary Material

Refer to Web version on PubMed Central for supplementary material.

Acknowledgments

We thank Susan L. Cohn (University of Chicago), M. Celeste Simon (University of Pennsylvania), and C Patrick Reynolds (Children's Oncology Group, Texas Tech University) for providing cell lines, and Rhea-Beth Markowitz for manuscript editing. Z. Dong is a VA senior Research Career scientist. The work was supported by a grant from NIH to H.-F. Ding (R01 CA190429) and by grants from the National Natural Science Foundation of China to Y. Xia (81702486) and to Y. Zha (81201981 and 81550031).

REFERENCES

1. Dang CV. MYC on the path to cancer. Cell 2012;149:22–35 [PubMed: 22464321]
2. Huang M, Weiss WA. Neuroblastoma and MYCN. Cold Spring Harbor perspectives in medicine 2013;3:a014415 [PubMed: 24086065]
3. Brodeur GM. Neuroblastoma: biological insights into a clinical enigma. Nat Rev Cancer 2003;3:203–16 [PubMed: 12612655]
4. Gessi M, von Bueren AO, Treszl A, Mühlen Az, Hartmann W, Warmuth-Metz M, et al. MYCN amplification predicts poor outcome for patients with supratentorial primitive neuroectodermal tumors of the central nervous system. Neuro-Oncology 2014;16:924–32 [PubMed: 24470553]
5. Pfister S, Remke M, Benner A, Mendrzyk F, Toedt G, Felsberg J, et al. Outcome prediction in pediatric medulloblastoma based on DNA copy-number aberrations of chromosomes 6q and 17q and the MYC and MYCN loci. J Clin Oncol 2009;27:1627–36 [PubMed: 19255330]
6. Williams RD, Chagtai T, Alcaide-German M, Apps J, Wegert J, Popov S, et al. Multiple mechanisms of MYCN dysregulation in Wilms tumour. Oncotarget 2015;6:7232–43 [PubMed: 25749049]
7. Rushlow DE, Mol BM, Kennett JY, Yee S, Pajovic S, Theriault BL, et al. Characterisation of retinoblastomas without RB1 mutations: genomic, gene expression, and clinical studies. Lancet Oncol 2013;14:327–34 [PubMed: 23498719]
8. Lee JK, Phillips JW, Smith BA, Park JW, Stoyanova T, McCaffrey EF, et al. N-Myc Drives Neuroendocrine Prostate Cancer Initiated from Human Prostate Epithelial Cells. Cancer Cell 2016;29:536–47 [PubMed: 27050099]
9. Dardenne E, Beltran H, Benelli M, Gayvert K, Berger A, Puca L, et al. N-Myc Induces an EZH2-Mediated Transcriptional Program Driving Neuroendocrine Prostate Cancer. Cancer Cell 2016;30:563–77 [PubMed: 27728805]
10. Beltran H, Rickman DS, Park K, Chae SS, Sboner A, MacDonald TY, et al. Molecular characterization of neuroendocrine prostate cancer and identification of new drug targets. Cancer Discov 2011;1:487–95 [PubMed: 22389870]
11. Hodgson JG, Yeh RF, Ray A, Wang NJ, Smirnov I, Yu M, et al. Comparative analyses of gene copy number and mRNA expression in glioblastoma multiforme tumors and xenografts. Neuro Oncol 2009;11:477–87 [PubMed: 19139420]
12. Brennan Cameron W, Verhaak Roel GW, McKenna A, Campos B, Noushmehr H, Salama Sofie R, et al. The Somatic Genomic Landscape of Glioblastoma. Cell 2013;155:462–77 [PubMed: 24120142]
13. Kim YH, Girard L, Giacomini CP, Wang P, Hernandez-Boussard T, Tibshirani R, et al. Combined microarray analysis of small cell lung cancer reveals altered apoptotic balance and distinct expression signatures of MYC family gene amplification. Oncogene 2006;25:130–8 [PubMed: 16116477]

14. Sos ML, Dietlein F, Peifer M, Schöttle J, Balke-Want H, Müller C, et al. A framework for identification of actionable cancer genome dependencies in small cell lung cancer. Proc Natl Acad Sci USA 2012;109:17034–9 [PubMed: 23035247]
15. Nau MM, Brooks BJ Jr., Carney DN, Gazdar AF, Battey JF, Sausville EA, et al. Human small-cell lung cancers show amplification and expression of the N-myc gene. Proc Natl Acad Sci USA 1986;83:1092–6 [PubMed: 2869482]
16. Dang CV, Reddy EP, Shokat KM, Soucek L. Drugging the 'undruggable' cancer targets. Nat Rev Cancer 2017;17:502–8 [PubMed: 28643779]
17. Ameri K, Harris AL. Activating transcription factor 4. The international journal of biochemistry & cell biology 2008;40:14–21 [PubMed: 17466566]
18. Kilberg MS, Shan J, Su N. ATF4-dependent transcription mediates signaling of amino acid limitation. Trends Endocrinol Metab 2009;20:436–43 [PubMed: 19800252]
19. Pakos-Zebrucka K, Koryga I, Mnich K, Ljujic M, Samali A, Gorman AM. The integrated stress response. EMBO reports 2016;17:1374–95 [PubMed: 27629041]
20. Zhang W, Yu Y, Hertwig F, Thierry-Mieg J, Zhang W, Thierry-Mieg D, et al. Comparison of RNA-seq and microarray-based models for clinical endpoint prediction. Genome Biol 2015;16:133 [PubMed: 26109056]
21. Puissant A, Frumm SM, Alexe G, Bassil CF, Qi J, Chanthery YH, et al. Targeting MYCN in neuroblastoma by BET bromodomain inhibition. Cancer Discov 2013;3:308–23 [PubMed: 23430699]
22. Huang DW, Sherman BT, Lempicki RA. Systematic and integrative analysis of large gene lists using DAVID bioinformatics resources. Nat Protocols 2008;4:44–57
23. Lee TI, Johnstone SE, Young RA. Chromatin immunoprecipitation and microarray-based analysis of protein location. Nat Protocols 2006;1:729–48 [PubMed: 17406303]
24. Mao L, Ding J, Perdue A, Yang L, Zha Y, Ren M, et al. Cyclin E1 is a common target of BMI1 and MYCN and a prognostic marker for neuroblastoma progression. Oncogene 2012;31:3785–95 [PubMed: 22120721]
25. Subramanian A, Tamayo P, Mootha VK, Mukherjee S, Ebert BL, Gillette MA, et al. Gene set enrichment analysis: a knowledge-based approach for interpreting genome-wide expression profiles. Proc Natl Acad Sci U S A 2005;102:15545–50 [PubMed: 16199517]
26. Cohn SL, Pearson ADJ, London WB, Monclair T, Ambros PF, Brodeur GM, et al. The International Neuroblastoma Risk Group (INRG) Classification System: An INRG Task Force Report. J Clin Oncol 2009;27:289–97 [PubMed: 19047291]
27. Maris JM. Recent Advances in Neuroblastoma. N Engl J Med 2010;362:2202–11 [PubMed: 20558371]
28. Marshall GM, Carter DR, Cheung BB, Liu T, Mateos MK, Meyerowitz JG, et al. The prenatal origins of cancer. Nat Rev Cancer 2014;14:277–89 [PubMed: 24599217]
29. Yang M, Vousden KH. Serine and one-carbon metabolism in cancer. Nat Rev Cancer 2016;16:650–62 [PubMed: 27634448]
30. Ducker GS, Rabinowitz JD. One-Carbon Metabolism in Health and Disease. Cell Metab 2017;25:27–42 [PubMed: 27641100]
31. Adams CM. Role of the transcription factor ATF4 in the anabolic actions of insulin and the anti-anabolic actions of glucocorticoids. J Biol Chem 2007;282:16744–53 [PubMed: 17430894]
32. Ye J, Mancuso A, Tong X, Ward PS, Fan J, Rabinowitz JD, et al. Pyruvate kinase M2 promotes de novo serine synthesis to sustain mTORC1 activity and cell proliferation. Proc Natl Acad Sci U S A 2012;109:6904–9 [PubMed: 22509023]
33. Ding J, Li T, Wang X, Zhao E, Choi JH, Yang L, et al. The Histone H3 Methyltransferase G9A Epigenetically Activates the Serine-Glycine Synthesis Pathway to Sustain Cancer Cell Survival and Proliferation. Cell Metab 2013;18:896–907 [PubMed: 24315373]
34. Zhao E, Ding J, Xia Y, Liu M, Ye B, Choi JH, et al. KDM4C and ATF4 Cooperate in Transcriptional Control of Amino Acid Metabolism. Cell Rep 2016;14:506–19 [PubMed: 26774480]

35. Liu M, Xia Y, Ding J, Ye B, Zhao E, Choi JH, et al. Transcriptional Profiling Reveals a Common Metabolic Program in High-Risk Human Neuroblastoma and Mouse Neuroblastoma Sphere-Forming Cells. Cell Rep 2016;17:609–23 [PubMed: 27705805]
36. Ben-Sahra I, Hoxhaj G, Ricoult SJ, Asara JM, Manning BD. mTORC1 induces purine synthesis through control of the mitochondrial tetrahydrofolate cycle. Science 2016;351:728–33 [PubMed: 26912861]
37. DeNicola GM, Chen P-H, Mullarky E, Sudderth JA, Hu Z, Wu D, et al. NRF2 regulates serine biosynthesis in non-small cell lung cancer. Nat Genet 2015;47:1475–81 [PubMed: 26482881]
38. Ma Y, Brewer JW, Diehl JA, Hendershot LM. Two distinct stress signaling pathways converge upon the CHOP promoter during the mammalian unfolded protein response. J Mol Biol 2002;318:1351–65 [PubMed: 12083523]
39. Chen H, Pan YX, Dudenhausen EE, Kilberg MS. Amino acid deprivation induces the transcription rate of the human asparagine synthetase gene through a timed program of expression and promoter binding of nutrient-responsive basic region/leucine zipper transcription factors as well as localized histone acetylation. J Biol Chem 2004;279:50829–39 [PubMed: 15385533]
40. Lin CY, Loven J, Rahl PB, Paranal RM, Burge CB, Bradner JE, et al. Transcriptional amplification in tumor cells with elevated c-Myc. Cell 2012;151:56–67 [PubMed: 23021215]
41. Nie Z, Hu G, Wei G, Cui K, Yamane A, Resch W, et al. c-Myc is a universal amplifier of expressed genes in lymphocytes and embryonic stem cells. Cell 2012;151:68–79 [PubMed: 23021216]
42. Xiao D, Yue M, Su H, Ren P, Jiang J, Li F, et al. Polo-like Kinase-1 Regulates Myc Stabilization and Activates a Feedforward Circuit Promoting Tumor Cell Survival. Mol Cell 2016;64:493–506 [PubMed: 27773673]
43. Brockmann M, Poon E, Berry T, Carstensen A, Deubzer HE, Rycak L, et al. Small molecule inhibitors of aurora-a induce proteasomal degradation of N-myc in childhood neuroblastoma. Cancer Cell 2013;24:75–89 [PubMed: 23792191]
44. Reynolds CP, Biedler JL, Spengler BA, Reynolds DA, Ross RA, Frenkel EP, et al. Characterization of human neuroblastoma cell lines established before and after therapy. J Natl Cancer Inst 1986;76:375–87 [PubMed: 3456456]
45. Pacold ME, Brimacombe KR, Chan SH, Rohde JM, Lewis CA, Swier LJ, et al. A PHGDH inhibitor reveals coordination of serine synthesis and one-carbon unit fate. Nat Chem Biol 2016;12:452–8 [PubMed: 27110680]
46. Mullarky E, Lucki NC, Beheshti Zavareh R, Anglin JL, Gomes AP, Nicolay BN, et al. Identification of a small molecule inhibitor of 3-phosphoglycerate dehydrogenase to target serine biosynthesis in cancers. Proc Natl Acad Sci USA 2016;113:1778–83 [PubMed: 26831078]
47. Reid MA, Allen AE, Liu S, Liberti MV, Liu P, Liu X, et al. Serine synthesis through PHGDH coordinates nucleotide levels by maintaining central carbon metabolism. Nature communications 2018;9:5442
48. Lau DT, Flemming CL, Gherardi S, Perini G, Oberthuer A, Fischer M, et al. MYCN amplification confers enhanced folate dependence and methotrexate sensitivity in neuroblastoma. Oncotarget 2015;6:15510–23 [PubMed: 25860940]
49. Ren P, Yue M, Xiao D, Xiu R, Gan L, Liu H, et al. ATF4 and N-Myc coordinate glutamine metabolism in MYCN-amplified neuroblastoma cells through ASCT2 activation. J Pathol 2015;235:90–100 [PubMed: 25142020]
50. Ding HF, Fisher DE. Induction of apoptosis in cancer: new therapeutic opportunities. Ann Med 2002;34:451–69 [PubMed: 12523501]

Significance:

This study identifies a MYCN-dependent metabolic vulnerability and suggests a coupled relationship between metabolic reprogramming and increased sensitivity to metabolic stress, which could be exploited for cancer therapy.

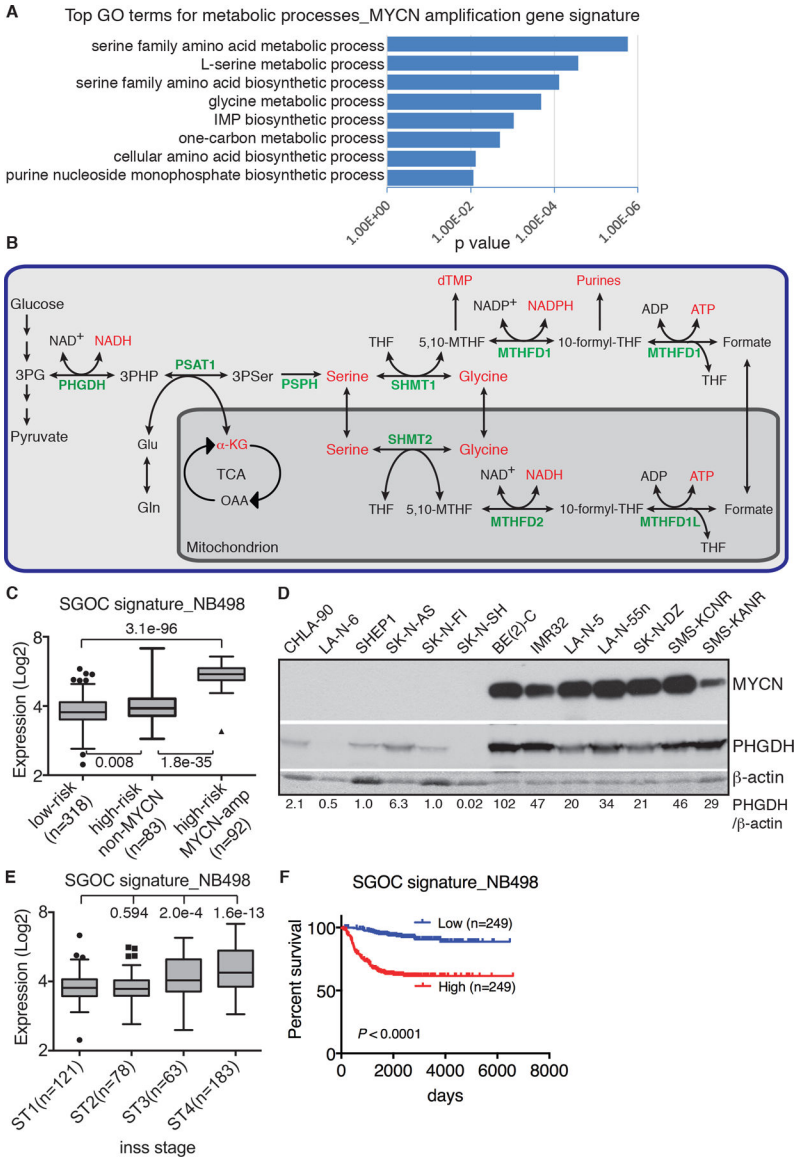

Figure 1.

Expression of the SGOC genes is upregulated in *MYCN*-amplified high-risk neuroblastoma. **A**, Top GO terms related to metabolic processes for the *MYCN*-amplification gene signature (n = 143). **B,** SGOC metabolic pathway with enzymes indicated in green and key products in red. **C,** Box plot of average mRNA expression of the SGOC 6-gene signature in relation to neuroblastoma risk groups and *MYCN* amplification status using the SEQC dataset. **D,** Immunoblotting of MYCN and PHGDH in neuroblastoma cell lines with or without *MYCN* amplification. PHGDH levels were quantified against β-actin, with the PHGDH level in SHEP1 cells being designated as 1.0. **E,** Box plot of average mRNA expression of the SGOC 6-gene signature in relation to neuroblastoma stages using the SEQC dataset. **F,** Kaplan-Meier survival curves for the SEQC cohort of 498 neuroblastoma patients based on the average mRNA expression of the SGOC 6-gene signature, with log-rank test *p* value

indicated. Unless otherwise indicated, data were analyzed with two-tailed Student's *t*-test, with *p* values indicated.

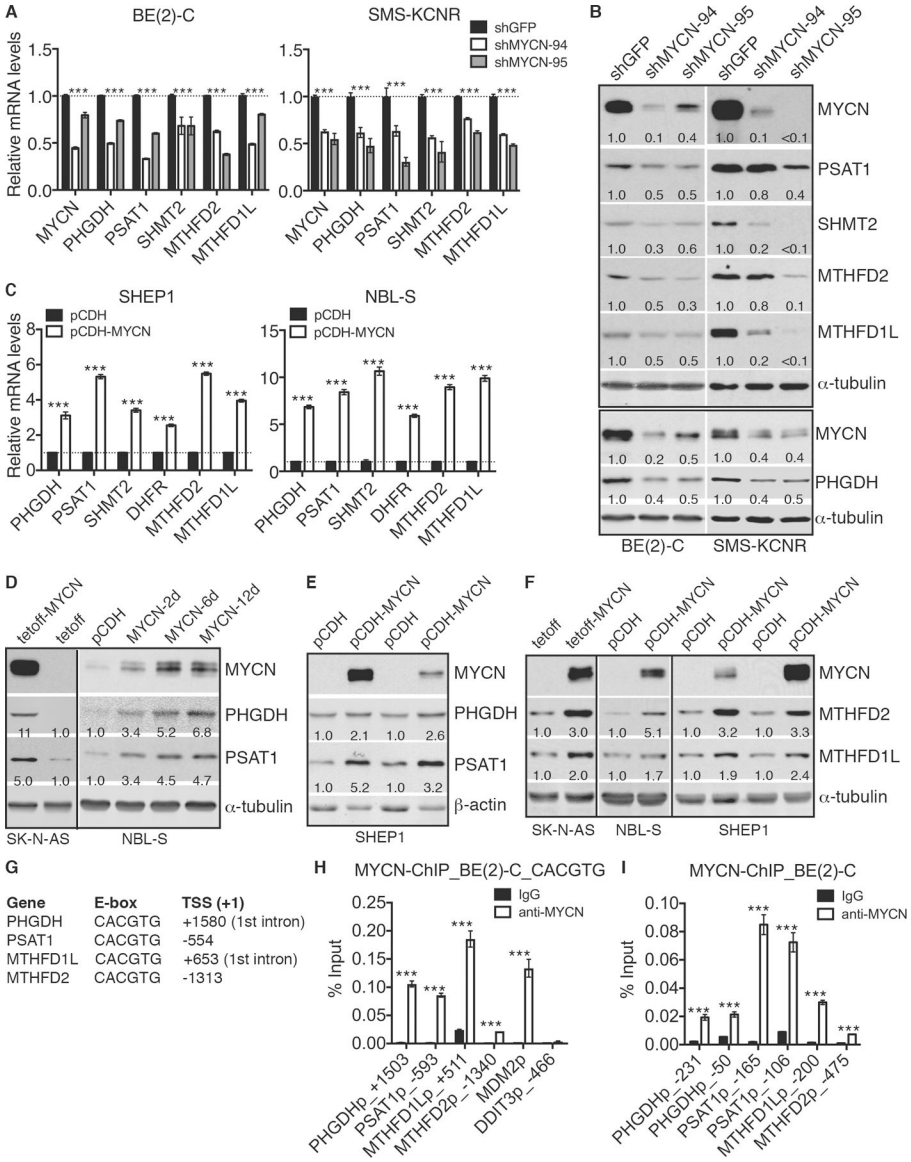

Figure 2.

MYCN transcriptionally activates the SGOC genes. **A-B**, qRT-PCR (**A**) and immunoblot (**B**) analyses of SGOC gene expression in *MYCN*-amplified cell lines expressing shRNA to GFP or MYCN. **C,** qRT-PCR analysis of SGOC gene mRNA expression in non-*MYCN*-amplified cell lines without (pCDH) or with (pCDH-MYCN) MYCN overexpression. **D-F,** Immunoblotting of SGOC enzymes in non-*MYCN*-amplified cell lines with constitutive (pCDH-MYCN) or inducible (tetoff-MYCN) MYCN expression. **G,** E-box sequences within the indicated SGOC genes relative to their transcription start site (TSS). **H-I,** ChIP-qPCR showing endogenous MYCN binding to the E-box sequences (**H**) and 5' regions (**I**) of the indicated SGOC gene promoters in BE(2)-C cells. The *MDM2* and *DDIT3* promoters were used as positive and negative control, respectively. Error bars represent SD (n = 3), and data were analyzed with two-tailed Student's *t*-test. Protein levels were quantified against α-tubulin or β-actin. ***$p < 0.001$.

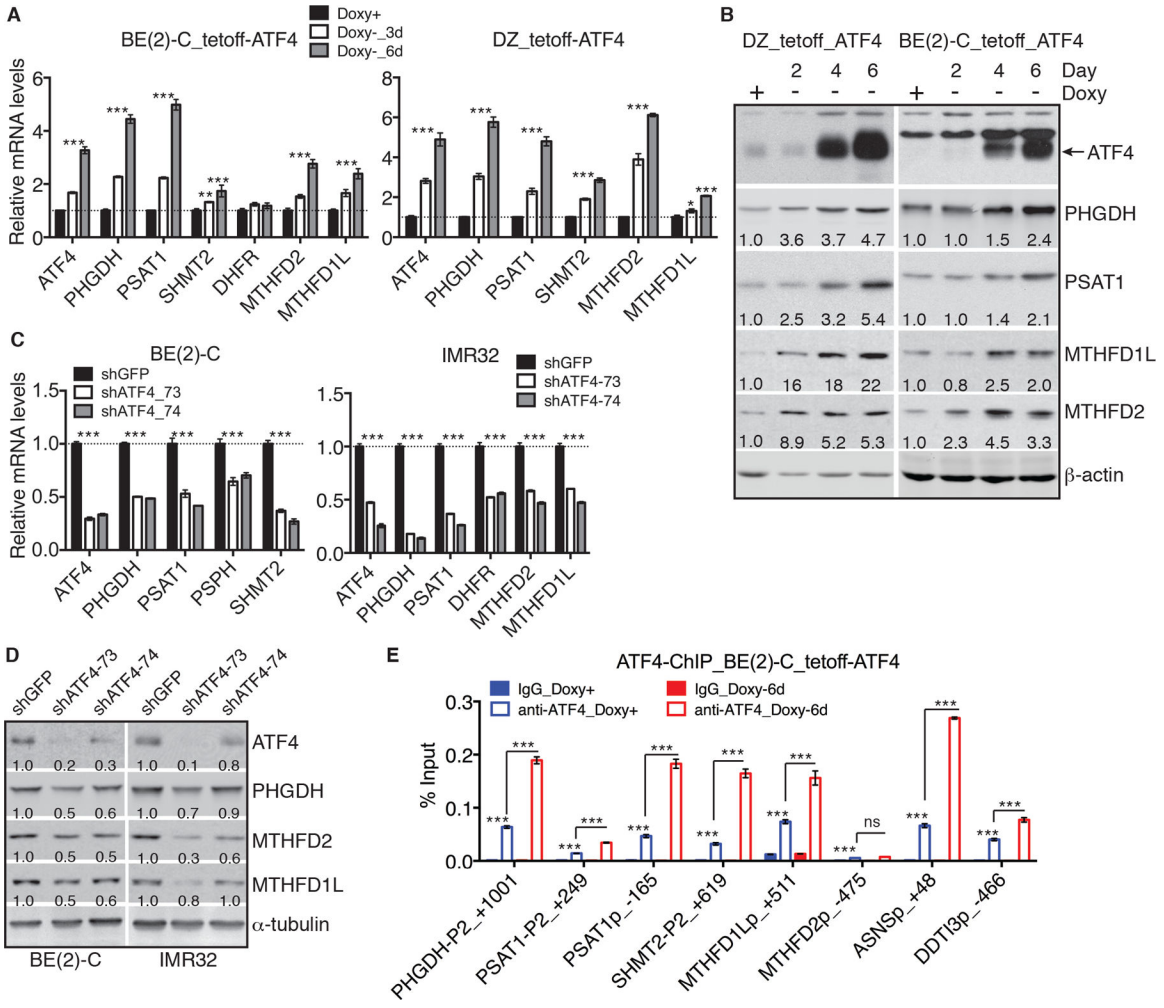

Figure 3.

ATF4 is a key transcriptional activator of SGOC gene expression in *MYCN*-amplified neuroblastoma cells. **A-B,** qRT-PCR (**A**) and immunoblot (**B**) analyses of SGOC gene expression in *MYCN*-amplified cell lines without (Doxy+) or with (Doxy-) ATF4 induction. **C-D,** qRT-PCR (**C**) and immunoblot (**D**) analyses of SGOC gene expression in *MYCN*-amplified cell lines expressing shRNA to GFP or ATF4. **E,** ChIP-qPCR showing ATF4 binding to the indicated SGOC gene promoters in BE(2)-C cells without (Doxy+) or with (Doxy-6d) ATF4 induction. The *ASNS* and *DDTI3* promoters were used as positive control. Error bars represent SD (n = 3), and data were analyzed with two-tailed Student's *t*-test. Protein levels were quantified against α-tubulin or β-actin. *$p < 0.05$, **$p < 0.01$, ***$p < 0.001$. ns, not significant.

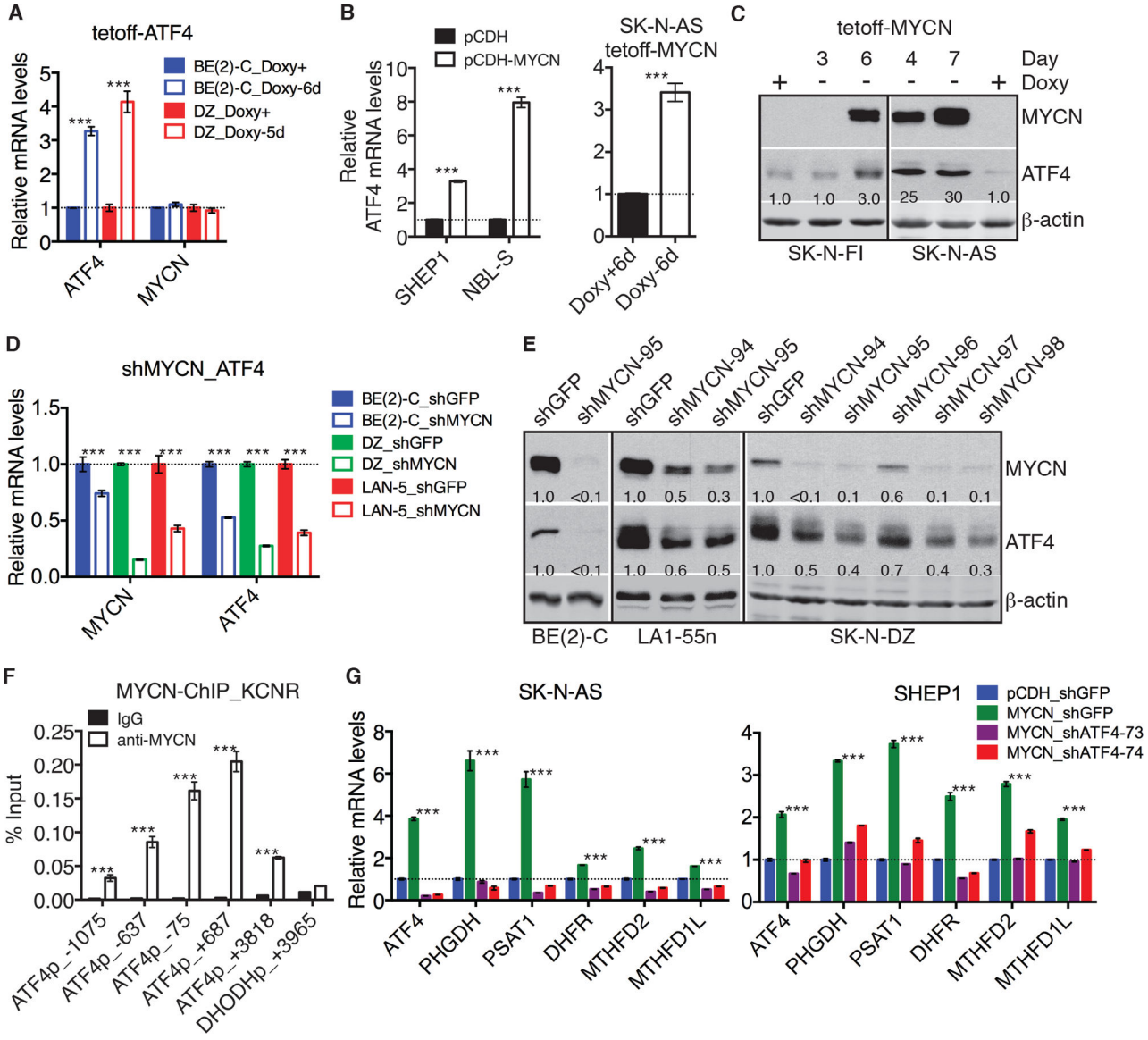

Figure 4.

ATF4 is a direct target gene of MYCN and is required for MYCN induction of the SGOC genes. **A,** qRT-PCR analysis of *ATF4* and *MYCN* mRNA expression in BE(2)-C and SK-N-DZ cells without (Doxy+) or with (Doxy-6d) ATF4 induction. **B-C,** qRT-PCR (**B**) and immunoblot (**C**) analyses of ATF4 mRNA and protein levels in non-*MYCN*-amplified cell lines with constitutive (pCDH-MYCN) or inducible (tetoff-MYCN, Doxy-) MYCN expression. **D-E,** qRT-PCR (**D**) and immunoblot (**E**) analyses of ATF4 mRNA and protein levels in *MYCN*-amplified cell lines expressing shRNA to GFP or MYCN. **F,** ChIP-qPCR showing endogenous MYCN binding to multiple sites in the *ATF4* gene in *MYCN*-amplified SMS-KCNR cells. The *DHODH* 3' region was used as negative control. **G,** qRT-PCR analysis of mRNA levels of *ATF4* and SGOC genes in vector (pCDH) or MYCN-overexpressing (MYCN) cell lines expressing shRNA to GFP or ATF4. Error bars represent

SD (n = 3), and data were analyzed with two-tailed Student's *t*-test. ATF4 and MYCN protein levels were quantified against β-actin. ***$p < 0.001$.

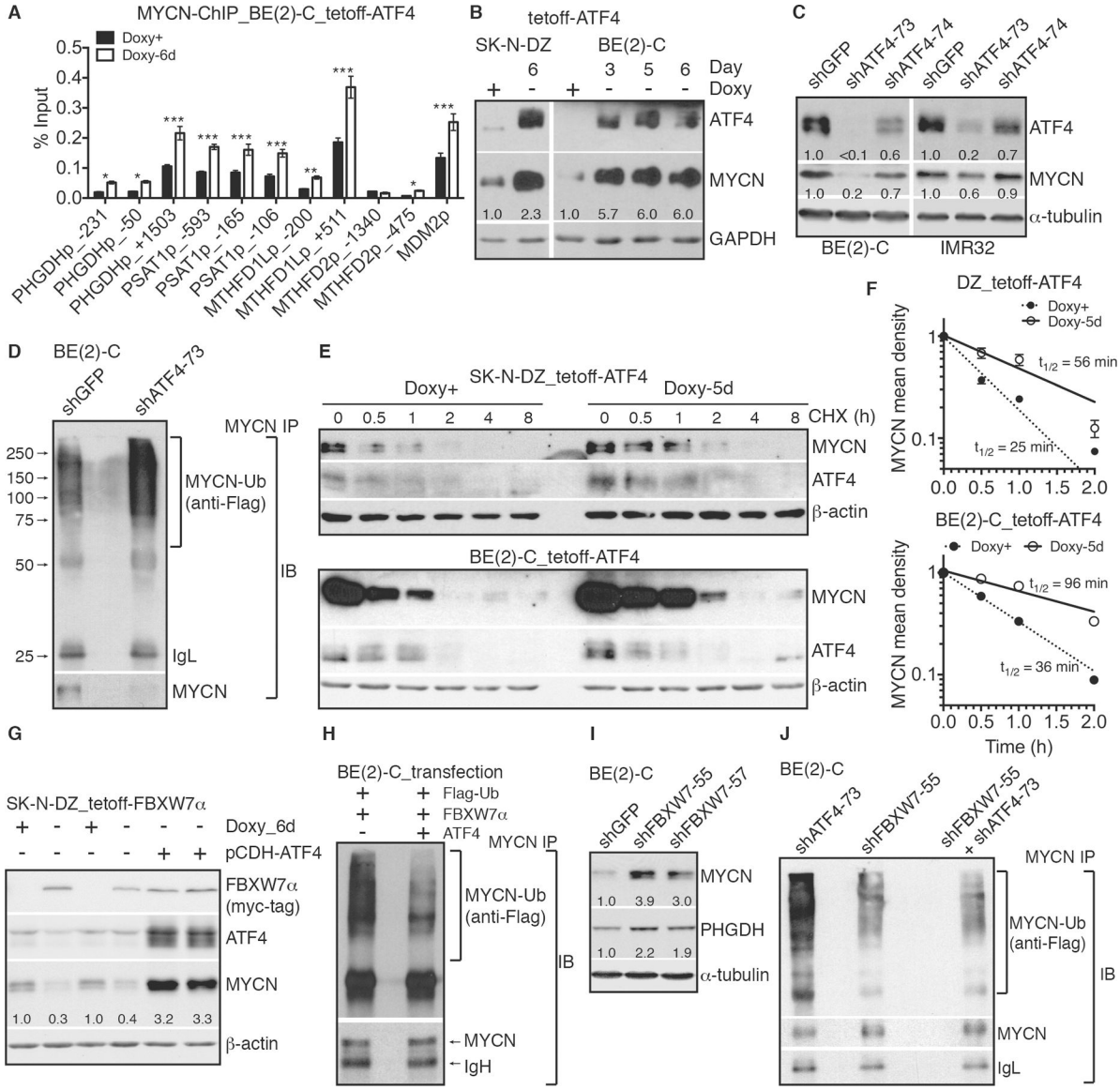

Figure 5.

ATF4 stabilizes MYCN protein. **A,** ChIP-qPCR showing increased MYCN occupancy at the SGOC gene promoters following ATF4 induction (Doxy-6d vs. Doxy+). **B,** Immunoblotting showing increased MYCN protein levels following ATF4 induction (Doxy- vs. Doxy+). **C-D,** Immunoblotting showing decreased MYCN protein levels (**C**) and increased MYCN ubiquitination (**D**) following ATF4 knockdown. IgL, immunoglobulin light chain. **E-F,** Immunoblotting (**E**) and quantification (**F**) of MYCN protein half-life in BE(2)-C and SK-N-DZ cells without (Doxy+) or with (Doxy-5d) ATF4 induction. Samples were collected at various time points following addition of cycloheximide (CHX). MYCN protein levels were quantified against β-actin and are presented as the fraction of the initial levels at time zero. **G,** Immunoblotting of the indicated proteins in SK-N-DZ cells without (Doxy+) or with (Doxy-6d) FBXW7α induction and ATF4 overexpression (pCDH-ATF4). **H,** Immunoblotting of MYCN ubiquitination in BE(2)-C cells transfected with plasmids

expressing Flag-ubiquitin, FBXW7α, and/or ATF4. IgH, immunoglobulin heavy chain. **I,** Immunoblotting showing increased MYCN and PHGDH protein expression following FBXW7 knockdown. **J,** Immunoblotting of MYCN ubiquitination in BE(2)-C cells infected with lentiviruses expressing shATF4–73, shFBXW7–55 or both. Error bars represent SD (n = 3), and data were analyzed with two-tailed Student's *t*-test. Protein levels were quantified against α-tubulin, β-actin, or GAPDH. $*p < 0.05$, $***p < 0.001$.

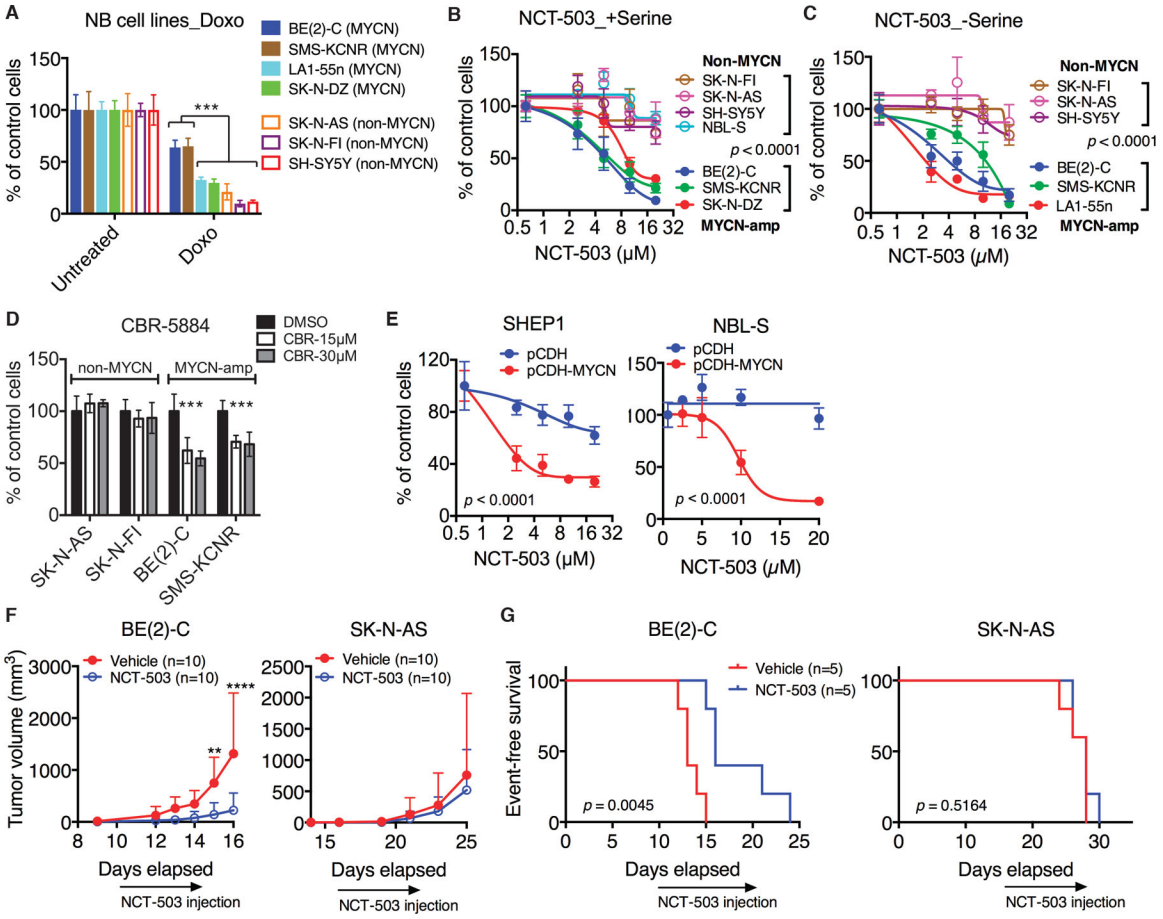

Figure 6.

MYCN sensitizes neuroblastoma cells to PHGDH inhibitors. **A,** Survival assays of neuroblastoma cell lines treated with doxorubicin (Doxo) at 0.5 μg/ml for 2 days. **B-D,** Survival assays of *MYCN*-amplified vs. non-*MYCN*-amplified cell lines treated with increasing concentrations of NCT-503 (**B, C**) for 2 days or CBR-5884 (**D**) for 3 days in the presence (**B, D**) or absence (**C**) of 0.4 mM serine. **E,** Survival assays of SHEP1 and NBL-S cells without (pCDH) or with MYCN (pCDH-MYCN) overexpression treated with increasing concentrations of NCT-503 for 2 days. **F-G,** Tumor growth (**F**) and event-free survival (**G**) curves for mice with BE(2)-C or SK-N-AS xenografts treated with vehicle or NCT-503 at 64 mg/kg for 10 days. Treatment started when tumors reached ~100 mm^3. Error bars in (**A-E**) represent SD (n = 4). Data were analyzed by two-tailed Student's *t*-test (**A, D**), two-way ANOVA (**B, C, E, F**) or Log-rank test (**G**). ***p* <0.01, ****p* < 0.001, *****p* < 0.0001.

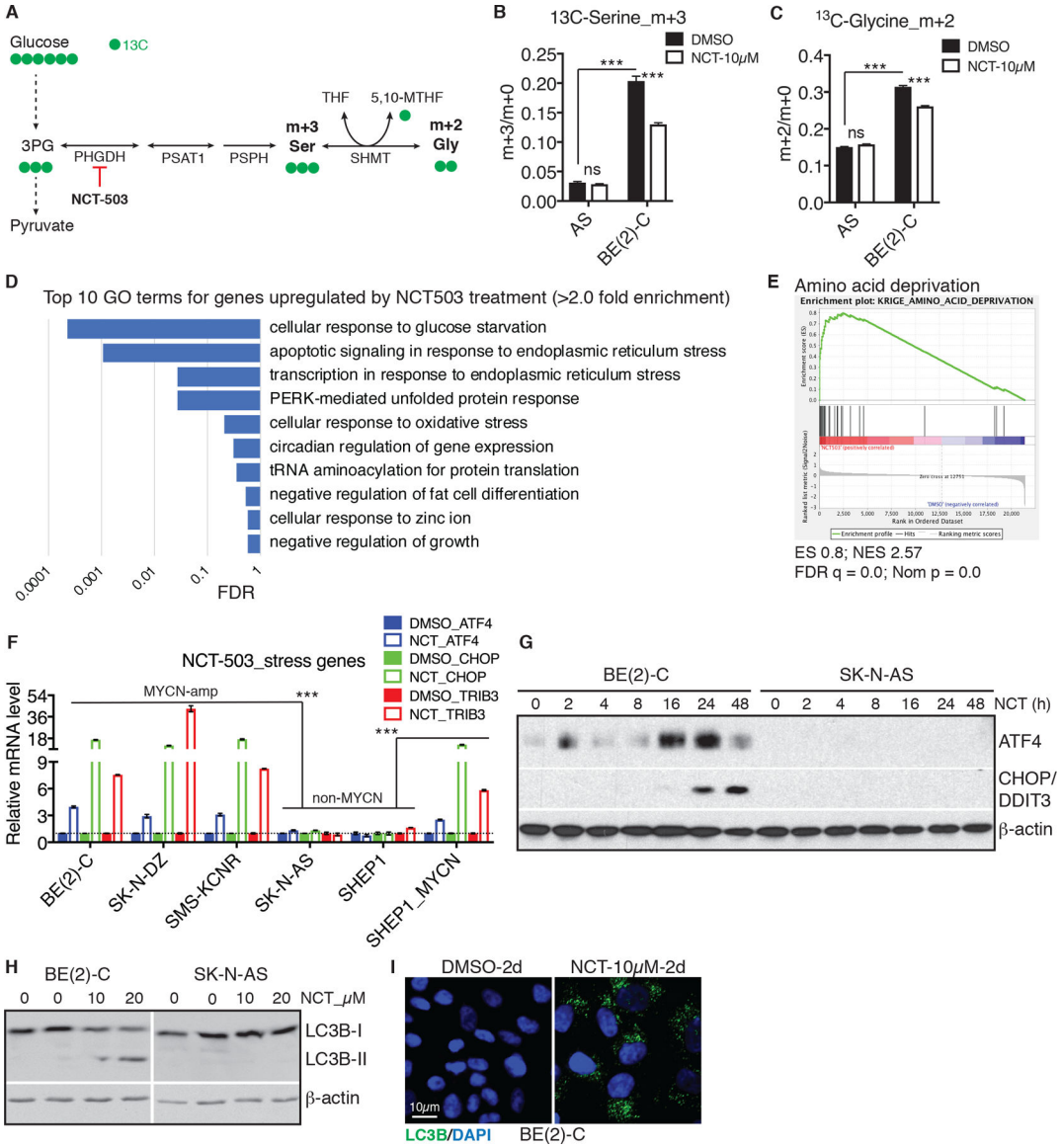

Figure 7.

PHGDH inhibition reduces glucose flux into the SGOC pathway and induces metabolic stress in *MYCN*-amplified cells. **A,** Diagram for incorporation of ^{13}C from glucose into serine and glycine. **B-C,** [U-^{13}C]glucose flux analysis in non-*MYCN*-amplified SK-N-AS and *MYCN*-amplified BE(2)-C cells treated with DMSO or 10 μM NCT-503 for 24 h. Shown are the ratio of ^{13}C-labeled m+3 serine or m+2 glycine to unlabeled serine or glycine. Error bars represent SD (n = 4–6 biological replicates). **D-E,** GO analysis of NCT-503-upregulated (**D**) and GSEA of NCT-503-responsive (**E**) genes in BE(2)-C cells treated with 10 μM NCT-503 for 48 h. **F,** qRT-PCR analysis of stress-responsive genes in *MYCN*-amplified and non-*MYCN*-amplified cell lines treated with DMSO or 10 μM NCT-503 for 48 h. Error bars represent SD (n = 3). **G,** Time-course analysis of ATF4 and CHOP (also known as DDIT3) protein expression in BE(2)-C and SK-N-AS cells treated with 10 μM NCT-503. **H,** Immunoblotting of LC3B in BE(2)-C and SK-N-AS cells treated

with the indicated concentrations of NCT-503 for 48 h. **I,** Immunofluorescence of LC3B-positive autophagosomes in BE(2)-C cells treated with 10 μM NCT-503 for 2 days. Data (**B, C, F**) were analyzed by two-tailed Student's *t*-test. ***$p < 0.001$.